An amplified femtosecond laser system for material micro-/nanostructuring with an integrated Raman microscope

Othman H. Y. Zalloum, Matthew Parrish, Alexander Terekhov, and William Hofmeister
The University of Tennessee Space Institute, 411 B.H. Goethert Parkway, Tullahoma, Tennessee 37388, USA

(Received 9 August 2009; accepted 26 April 2010; published online 27 May 2010)

In order to obtain new insights into laser-induced chemical material modifications, we introduce a novel combined approach of femtosecond pulsed laser-direct writing and *in situ* Raman microscopy within a single experimental apparatus. A newly developed scanning microscope, the first of its kind, provides a powerful tool for micro-/nanomachining and characterization of material properties and allows us to relate materials' functionality with composition. We address the issues of light delivery to the photomodification site and show the versatility of the system using tight focusing. Amplified femtosecond pulses are generated by a Ti:sapphire laser oscillator and a chirped-pulse regenerative amplifier, both pumped by a diode-pumped frequency doubled neodymium-doped yttrium orthovanadate ($Nd:YVO_4$) laser operating at 532 nm. Results of Raman spectroscopy and scanning electron microscopy images of femtosecond laser micro-/nanomachining on the surface and in the bulk of single-crystal diamond obtained from first trials of this instrument are also presented. This effective combination could help to shed light on the influence of the local structure fluctuations on controllability of the laser processing and the role of the irradiation in the ablation processes ruling out possible imprecisions coming from the use of the two independent techniques. © *2010 American Institute of Physics.* [doi:10.1063/1.3430073]

I. INTRODUCTION

Ultrashort laser pulses show great potential for precise micro-/nanomachining.[1–3] Femtosecond laser micro-/nanomachining is a consequence of laser-induced optical breakdown, a process by which optical energy is transferred to the material, ionizing a large number of electrons that, in turn, transfer energy to the lattice.[4] As a result of the irradiation, a variety of processes can be identified, among them color center formation, phase, or structural modification, leaving behind a localized permanent change in the refractive index or even a void. The technique utilizes the ultrashort laser pulse properties to achieve control in shaping the desired microstructures with minimal collateral damage to the surroundings. The laser energy can be deposited efficiently, rapidly, and localized in practically any material, whether transparent or opaque. The main features of material processing with femtosecond laser pulses are (i) efficient, fast, and localized energy deposition, (ii) well-defined deformation and ablation thresholds, and (iii) minimal thermal and mechanical damage of the substrate material. With the general push to smaller structures, the prospects for this technique are very promising.[5]

In parallel, conventional Raman microscopy[6–10] is currently applied to the analysis of a large number of industrially important films and coatings and can be used for the identification of impurities and defects and for the characterization of materials themselves.[11–13] In addition to its spatial resolution, which adds to its usefulness for investigating femtosecond ablated films, Raman spectroscopy can distinguish the various forms of carbon. The Raman C–C band intensities in the 1300–1700 cm^{-1} region are enhanced due to the resonant Raman effect. Thus, carbon with sp^3-type bonding (diamond) or sp^2-type bonding (graphite and carbonaceous materials) can be characterized. Single crystal diamond and perfect graphite are each characterized by a single Raman line which appears at 1332 and 1580 cm^{-1}, respectively. However, if the graphite lattice is disordered, a second line appears at 1360 cm^{-1} which grows in sp^3 bonds. Diamondlike carbon (DLC) is also an important amorphous carbon or hydrogenated amorphous carbon thin film material with a high fraction of metastable sp^3 carbon bonding. Raman spectra of DLC are broad and differ notably from those of graphite and amorphous carbon. Two particular bands in the 1300–1700 cm^{-1} region, the D (so-called disorder) and G (graphitic) bands, often show changes in their peak location and intensity depending on the structure of the carbon.[14]

An important, but not fully exploited, finding of Raman analysis is that femtosecond ablated films and debris generated during the ablation process may have distinctly different composition and features than the original materials or coatings themselves. For example, for certain applications such as cutting by femtosecond laser pulses, graphitization of diamond can be a primary concern. On the contrary, diamond graphitization can be of particular interest in three-dimensional laser microstructuring of diamond due to the possibility of creating local graphitized regions in the bulk, provided that the mechanical stresses generated as a result of the bulk graphitization do not cause local mechanical damage in diamond crystals as demonstrated by other groups.[15] Raman spectroscopy can provide new insights into the graphitization process, the influence of the local structure fluctuations on controllability of the laser processing, and the role of the irradiation in the ablation processes.

The Raman technique is also often used as a rapid nondestructive method for the control of processed silicon. This analysis is based on the observation of the position of the silicon band at approximately 520 cm^{-1}, which is very sensitive to local lattice characteristics. Still with reference to the shift in the 520 cm^{-1} band, compressive or tensile stress can be evaluated; this parameter can be determined as a function of the position. Other examples include (a) the examination of femtosecond pulse interaction with industrial polymers in terms of defect identification and characterization of molecular orientation and crystallinity[11] and (b) performing a series of Raman measurements as a layered sample is ablated in depth. For these reasons, *in situ* Raman can provide important and new insights in laser-induced chemical material modifications.

In this paper we describe a combined instrumental technique for amplified femtosecond pulsed laser-direct writing integrated with micro-Raman microscopy. The design of the scanning microscope is based on providing a robust, flexible, rugged integrated instrument that could take the typical "research" abuse and maintain its optical alignment. The instrument's modular construction allows for future modification and allows improving functionality or alteration of its present performance. The system is flexible and can be applied to both absorptive and transparent substrates. We address the issues of light delivery to the photomodification site and show the versatility of the system using tight focusing on diamond materials.

II. MATERIALS AND METHODS

A. Experimental setup

A block diagram illustrating the generation of the amplified femtosecond pulses is shown in Fig. 1. Amplified femtosecond pulses are generated by a system consisting of Tsunami oscillator (Spectra Physics—model 3941) seeding a RegA 9000 (Coherent, Inc.) regenerative amplifier, both of which are pumped with cw green solid-state Verdi-18 laser (Coherent, Inc.). Femtosecond pulses are directed to a scanning microscope consisting of a fabrication workstation and an integrated Raman microscope. In the microscope workstation, the sample is mounted on a piezoelectric nanostage (Mad City Laboratories, Inc.), which is positioned on a large range of *XY* motion microstage (McBain, Inc. precision stages and Compumotor, Inc. stepper motors with National Instruments motor drivers) to cover large areas of the sample. The stage is moved in a preprogrammed *x*, *y* pattern under LabVIEW control.

An externally triggered shutter controlled the ablation time for the 250 kHz repetition rate experiments. A neutral density filter placed within the beam path was used to adjust the power at the sample. The laser beam was focused on the front surface of the samples by a microscope objective with numerical apertures (NAs) of 0.65, 0.9, or 1.2. The objective was mounted on a stage with adjustable *Z* direction. The delivery system allowed direct viewing during material ablation through a 10× eyepiece and a high resolution digital

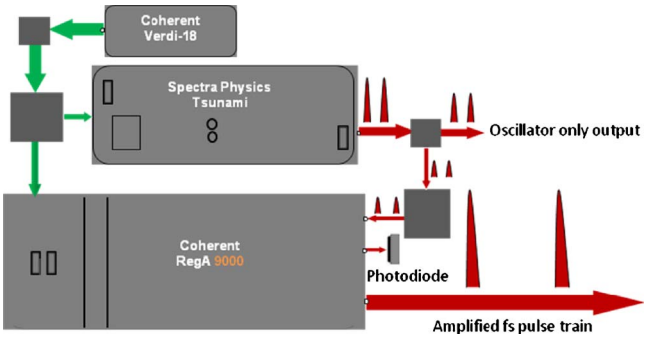

FIG. 1. (Color online) Amplified femtosecond pulses are generated with a system consisting of Tsunami oscillator (Spectra Physics-model 394, modified to operate at 76 MHz) seeding a RegA 9000 (Coherent, Inc.) regenerative amplifier, both of which are pumped by a diode pumped frequency doubled neodymium-doped yttrium orthovanadate ($Nd:YVO_4$) laser operating at 532 nm (Verdi V18, Coherent, Inc.). Also shown is the oscillator only output. The photodiode is connected to an oscilloscope to display the repetition rate and the status of the amplified femtosecond pulse train.

camera. The system is located in a Class-1000 clean at a controlled constant room temperature on a vibration isolation table.

A central personal computer controls digital delay and pulse generation for pulse type single shot or high repetition rates, shutter control for ablation duration, and nanostage and motion control unit for positioning features on the sample. The motion control units include (a) a nanostage controller (MCL NanoDrive) which is a complete electronic package for subnanometer positioning. It features low noise, low drift amplifiers, absolute position control, bandwidth selection, and closed loop feedback which is essential for high-repeatability and subnanometer resolution for a nanopositioner. Closed loop feedback ensures that the displacement as a function of input voltage is highly linear and free of positioning errors caused by inherent creep and hysteresis in the piezoactuators, (b) a four-axis and stepper motor drive unit (National Instruments MD-76040) that incorporates an efficient bipolar chopper architecture that converts step and direction control signals into winding currents for two-phase stepper motors. Because the MD-7604 driver supplies constant current to the step motor, the load-velocity-current response curves fit the classical representation for step motors.

Two iris diaphragms serve to define the femtosecond beam. The low energy pulses available from the oscillator are amplified to microjoules of energy. At the base of the pump control optical assembly, the Verdi-18 pump beam is divided into 6 W to pump the oscillator and 12 W to pump the regenerative amplifier. The pump beam is directed into the oscillator with a beam splitter and two turning mirrors.

Beam tubes enclose the laser path and prevent mirror contamination and beam pointing by stray air currents. The 6 W Tsunami pump beam is directed to the titanium sapphire crystal in the normal Tsunami pump geometry. In this arrangement the Tsunami laser is in femtosecond mode locked operation and produces an ultrafast train with 500 mW average output power that passes through a beam splitter through a short beam tube. A typical pulse width is 60 fs. A 150 mW reflected pulse train from the beam splitter at the Tsunami output is fed into RegA 9000 amplifier with two turning

mirrors and injected into the amplifier cavity with a TeO_2 (tellurium dioxide) acousto-optic cavity dumper. A 76 MHz photodiode signal from the oscillator is used to generate a 38 MHz master clock for the timing of all the RegA 9000 rf pulses. An electronic control system is available to deliver complete timing control of pulse injection, dumping, and gain-switching elements, providing a real-time liquid crystal display of amplifier performance and the ability to memorize and reset any system parameter. Amplification over 25 roundtrips allows the dispersion within a TeO_2 Q switch in the RegA 9000 to expand this pulse to several microjoules of energy. The amplification of the laser pulse inside the RegA 9000 cavity is measured in RegA head routed to the RegA controller and is also supplied for display on an oscilloscope. The accumulated chirp acquired by the pulses in amplification is canceled with a simple single-grating compressor. At greater than 50% efficiency the compressor produces microjoule pulses with autocorrelation pulse widths of less than 300 fs full width at half maximum. The average output power (P_{av}) from RegA 9000 is determined by the pump power available. Several watts of cw optical power are typically available from the amplifier. For pulsed operation, a cw pumped laser is limited only by the laser storage time of the gain medium. In titanium:sapphire at room temperature, this storage time (T_s) is approximately 2.5 μs. The maximum pulsed energy (E_p) is given by $E_P = P_{cw} T_s$ and is valid at repetition rates up to approximately $1/(3T_s) = 130$ kHz for titanium:sapphire. For higher repetition rates (R) the energy is typically reduced and follows the general form[16]

$$E_P = P_{cw} T_s \left[1 - \exp\left(\frac{-1}{T_s R} \right) \right]. \quad (1)$$

At $R = 250$ kHz the pulse energy, E_p is reduced to 80% of maximum value while the average power is 50% of the cw average power. At 250 kHz, if the average power is 1.0 W, the output energy $E = P_{av}/R = 4$ μJ. This is where the RegA 9000 is routinely operated. The amplifier can be externally triggered to produce single pulses.

The system model that best represent the various microscope units of our system is shown in Fig. 2. After exiting two iris diaphragms used to define the beam, the femtosecond pulses are delivered to the scanning microscope by using a periscope assembly (PA), which provides a convenient way to redirect and change the elevation of a beam. The PA consists of a pair of 45° mirrors with lockable adjustment knobs to provide 360° of rotation of the incoming light. The upper housing also provides a microstage for fine control, which can be used to precisely deliver the input beam to the proper position on the dichroic filter mirror for subsequent reflection into the pupil of the objective. The dichroic filter mirror is optimized for reflecting the 800 nm laser line incident at 45° and is mounted on a rotatable platform inside a cage cube with kinematic adjustments. This is particularly important to ensure proper alignment of the filter mirror in the cube. Prior to being locked down, the beam splitter can also be freely rotated through 360° while inside the cage cube. The base platform has three adjusters to provide pitch, roll, and Z translation in addition to rotational positioning. The cages are attached to a revolving turret that is rotated into the optical train when required as shown in Fig. 2(b). This method enables rapid changeover between femtosecond machining and Raman spectroscopy.

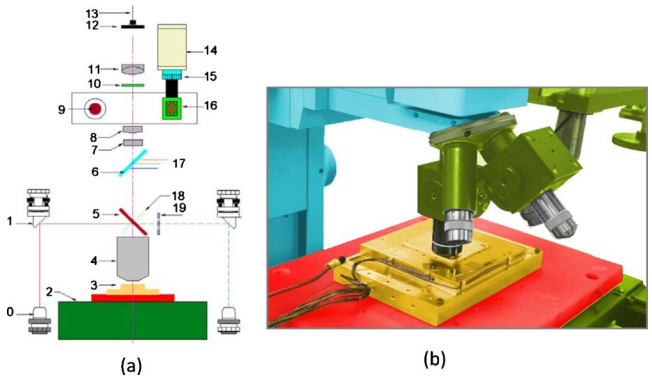

FIG. 2. (Color online) (a) The optical system model that represents the fabrication workstation and the integrated Raman microscope. The microscope employs infinity corrected optics and is fitted with a vertical illuminator. Light passing through the objective lens emerges and propagates from the objective as a parallel beam of infinite focus. The PA provides a convenient way to redirect and change the elevation of a beam, and consists of a pair of 45° mirrors (0) and (1) with lockable adjustment knobs to provide 360° of rotation of the incoming light. The upper housing also provides fine control, which can be used to compensate for angular deviations of the input beam, (2) is a x-y microstage, (3) xyz nanostage, (4) infinity corrected microscope objective, (5) 800 nm dichroic filter mirror, (6) half mirror, (7 and 8) tube lenses, (9) eyepiece, (10) long wave pass Raman edge filter, (11) focusing lens, (12) fiber optic endplate, (13) multimode fiber, (14) 12 bit digital camera, (15) 9 mm computer television lens, (16) 45° mirror, (17) white light illumination produced from a reflected light vertical illuminator, (18) 532 nm dichroic filter mirror, and (19) 532 nm narrow bandpass filter. (b) Isometric view showing the nanostage and the microscope turret and its attachments, two dichroic filter mirrors mounted on a rotatable platform inside cage cubes with kinematic adjustments are used to reflect the needed wavelength of light to be projected on the sample for either Raman spectroscopy (532 nm) or femtosecond machining (800 nm).

The Raman excitation pump is derived from the Verdi-18 solid state laser operating at 532 nm and is delivered to the microscope using a second PA as described above. The 532 nm laser beam then passes through a narrow bandpass filter with high transmission (exceeding 90% at the laser wavelength) while rapidly rolling off to an optical density (OD) >5 at wavelengths differing by only 1% from 532 nm, and OD >6 at wavelengths differing by only 1.5% from the laser wavelength. This filter is mounted in a short tube at the entrance of the cage cube. The collimated laser beam is reflected by the dichroic filter mirror and focused onto the sample with an infinity corrected microscope objective. The incident and backscattered light fills the objective lens pupil. The Raman dichroic filter mirror reflects the 532 nm laser line incident at 45° while transmitting longer Raman-shifted wavelengths with an ultrasteep transition width of $<1\%$ of the laser wavelength (regardless of polarization). The Raman-backscattered light is then collected by the same microscope objective and brought to focus onto the core of a multimode optical fiber after being passed through a long wave pass Raman edge filter with a transition width <186 cm^{-1}, thus allowing deep laser line blocking. The fiber core (400, 100, or 50 μm) acts as a pinhole.

The multimode fiber is coupled to a research grade spectrometer (Ocean Optics, Inc., model QE65000) which is equipped with a thermoelectric-cooled and back-illuminated charge-coupled device detector. The two-dimensional area detector can achieve up to 90% quantum efficiency. The spectrometer enables low-light-level detection and long integration times from 8 ms to 15 min. As a result, the dynamic range can be increased significantly. The stray light is $<0.08\%$ at 600 nm; 0.4% at 435 nm (manufacturer specified). Wavelength calibration coefficients are programed into a memory on the spectrometer.

The microscope is also equipped with a reflected light vertical illuminator (not shown) to direct light emitted by the lamp onto the specimen. The light beam emitted from the vertical illuminator is reflected by the half mirror, transmitted through the objective, and then illuminates the specimen. The light reflected on the specimen is transmitted back through the objective and the half mirror. Then it is made to form the image of the specimen at an intermediate image position by the tube lens. Besides its internal optics, the vertical illuminator also contains slider frames for filters that can be employed to select the desired wavelength and/or adjust the overall intensity of lamp's light passing through the system. The slider frames allow the filters to be quickly inserted and removed from the light path while viewing the specimen surface. The vertical illuminator also contains an aperture and field diaphragm combination, both of which have variable iris apertures that dictate the field size and illumination intensity. Centering of the aperture and field diaphragms and other alterations to the iris size are accomplished by adjusting a pair of knobs located on the exterior side of the vertical illuminator housing.

In place of one of the eyepieces, we installed a high resolution digital camera (C8484–05, Hamamatsu) with a wide dynamic range of 12 bit digital output and high sensitivity in the visible to infrared region to provide digital imaging of a specimen's surface at low light levels. This capability is necessary for proper sample location and to monitor the operation. The camera provides a preview image and is a precise focusing aid for femtosecond machining applications. The camera is directly controlled by the computer, which is equipped with a Camera Link frame grabber (National Instruments PCI-1426) to acquire images. Image brightness is proportional to the square of the NA and inversely proportional to the square of the total magnification. The brightest images are gathered by an objective with high NA and low magnification. Typically, the amount of change in magnification will be more than the amount of change in NA—meaning magnification will play a stronger role in image brightness. Higher magnification images will typically be darker than lower magnification images. Depth of field—the distance above and below the focal plane that is still seen as acceptably sharp—will be affected by the NA of the lens and the wavelength of the illumination (proportional to λ/NA^2). If NA is increased to improve resolution, the depth of field will be decreased.

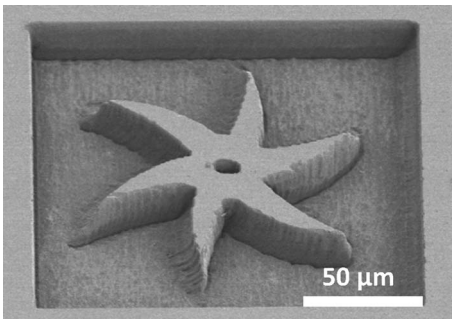

FIG. 3. Curved structures machined on the surface of HPHT single-crystal diamond at a laser pulse energy of 1.2 μJ.

B. Materials

In these experiments, we have used synthetic diamond materials. The single-crystal diamonds were supplied by the Diamond Edge Co. of Largo, Florida and were created by a high pressure, high temperature (HPHT) process. This material is transparent at the laser operating wavelength of 800 nm. The second diamond material is created by low pressure chemical vapor deposition (LPCVD). This material has a high content of sp^2 bonds and absorbs at the laser operating wavelength of 800 nm.

III. EXPERIMENTAL RESULTS AND DISCUSSION

Various desired shapes and configurations can be fabricated when the sample is translated with the focused laser beam incident on the surface of the sample. The structure shown in Fig. 3 was machined on the surface of a HPHT single-crystal diamond at a laser pulse energy of 1.2 μJ. Prior to machining, all the samples were cleaned with acetone and methanol (for 3 min with each) in an ultrasonic cleaner and dried with nitrogen. The depth of features was estimated to be 24.7 μm. This robust structure has well-defined features and shows the possibility of machining curved features with high degree of repeatability. It is interesting to note that the ablation process induced nanoscale surface morphologies in the irradiated area that results in a reduced Raman intensity due to scattering by this modified surface as shown in Figs. 4 and 5.

Single crystal diamond and perfect graphite are each characterized by a single Raman line which appears at 1332 and 1580 cm^{-1}, respectively. However, if the graphite lattice is disordered, a second line appears at 1360 cm^{-1} which grows in sp^3 bonds.[14] Using Raman spectroscopy we find that under respective laser parameters the graphite peaks are absent and the diamond structures retain the original diamond composition as demonstrated in Fig. 5. The reduced Raman signals in the irradiated areas are due to scattering by the periodic ripples formed in such a modified surface. It should be noted that the ablated sample was cleaned for 3 min in acetone followed by another 3 min in methanol in an ultrasonic bath prior to Raman measurements.

The spontaneous formation of periodic ripples on the surface of a material illuminated with polarized pulsed laser light has been reported in many different materials. The period and orientation of these surface ripples, known in the

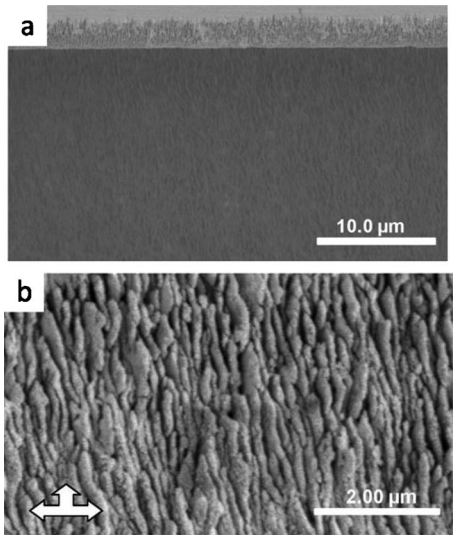

FIG. 4. (a) SEM images of the HPHT synthetic single-crystal diamond surface showing a middle rectangular area after irradiation with a pulse train of 200 fs laser pulses at a rate of 250 kHz with a pulse energy of 840 nJ. The figure also demonstrates that ablation induces nanoscale surface morphology in the irradiated area which results in a reduced Raman intensity due to scattering by this modified surface. (b) Magnified SEM image of the irradiated area in (a). The laser polarization is oriented horizontally perpendicular to the translation direction.

literature as laser-induced periodic surface structures, mainly depend on the angle of incidence, polarization, frequency, and energy of the laser beam.[1,17]

In what follows, we use examples showing what can be done with the combined system that could allow a significant improvement in previous measurements. In these examples we machined a "square-diamond" pattern and an "edge" pattern of the "square-diamond" pattern machined on a LPCVD diamond surface. We believe that this combined system may help to rule out possible imprecisions coming from the use of the two independent techniques for such and similar patterns. In addition to creating features on various materials, the experimental setup allows micro-Raman measurements to be carried out on the exact path used for the ablation while carefully coordinating the alignment and positioning of these features through software-controlled stages with nanometer precision.

The variation in laser processing parameters allows fabrication of a wide range of structural designs with specific properties on the surface or in the bulk of a diamond. Careful selection of laser machining parameters produces well-defined microstructures. Patterns of lines can be formed by ablating with a large number of consecutive pulses along a single column, forming continuous structures. Figure 6 shows an optical microscope image of an "edge" pattern of a "square-diamond" pattern machined on the LPCVD diamond surface. This pattern was generated by irradiating the surface of the LPCVD sample with a pulse train of 200 fs laser pulses at a rate of 250 kHz with a pulse energy of 13.2 nJ. Unless otherwise specified, when making shapes or two-dimensional arrays of holes, the translation stage was programed to move in a back and forth pattern at predefined intervals. During this motion, the laser polarization was in the plane of the translation stage and perpendicular to the translation direction. If the first column of the grid is scanned along the *y* axis from forth to back, then when the edge of the shape is reached, the translation stage is moved to the

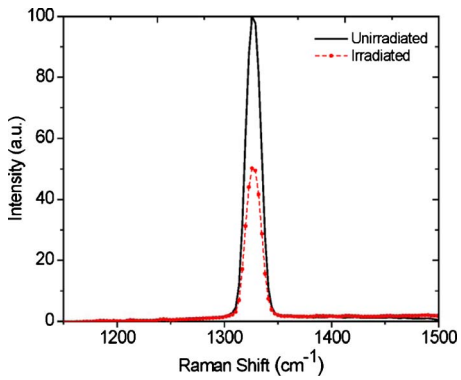

FIG. 5. (Color online) Micro-Raman spectra of the unirradiated and irradiated areas of a laser-processed HPHT synthetic single-crystal diamond sample. It exhibits the characteristic single line near 1332 cm^{-1}.

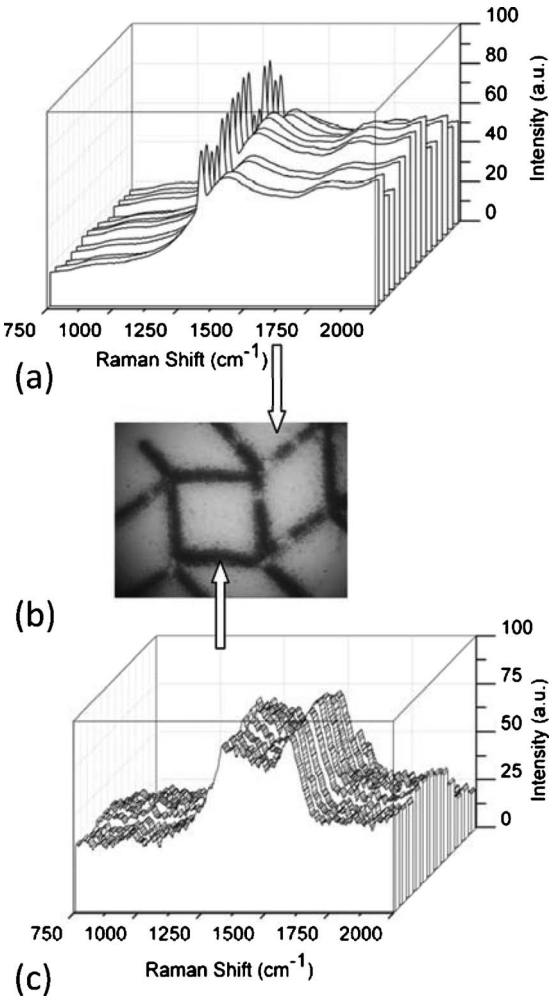

FIG. 6. Development of the graphitization generated by irradiating the surface with a pulse train of 200 fs laser pulses at a rate of 250 kHz with a pulse energy of 13.2 nJ. (a) and (c) show micro-Raman spectra of the unirradiated and irradiated area, respectively, of the laser-processed LPCVD synthetic diamond sample. (b) is a magnified optical microscope image of the laser processed sample. In (c) Raman spectra of the ablated pattern before removing debris showing two graphite peaks; the D peak at ~1360 cm^{-1} and the G peak at ~1580 cm^{-1}.

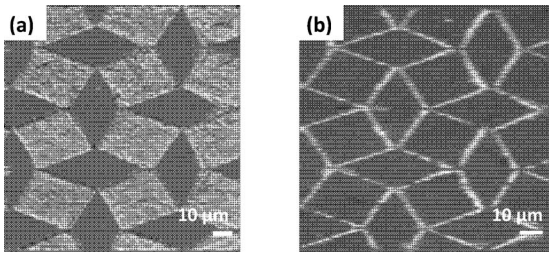

FIG. 7. (a) SEM images of the LPCVD diamond surface showing a "square-diamond" pattern. The squares are irradiated with a pulse train of 200 fs laser pulses at a rate of 250 kHz with a pulse energy of 40 nJ. (b) SEM image of the square-diamond "edge" pattern is generated by irradiating the surface with a pulse train of 200 fs laser pulses at a rate of 250 kHz with a pulse energy of 13.2 nJ. The laser polarization is oriented horizontally perpendicular to the translation direction.

next column by moving along the laser polarization (x axis). The second column of the shape is also scanned from forth to back. This column-by-column process continues until the entire shape or array of holes has been formed. During ablation, the microstage was inactive and the nanostage was operated at 11 μm s^{-1} to create the micropatterns.

This first set of Raman measurements was carried out immediately after ablation before removing any debris. The Raman spectra of the unirradiated regions of the sample are shown in Fig. 6(a). The spectra exhibit the characteristic single line near 1332 cm^{-1} and background peaks above ~1400 cm^{-1}. The Raman spectra of the ablated pattern before removing debris are shown in Fig. 6(c) showing two graphite peaks; the D peak at ~1360 cm^{-1} and the G peak at ~1580 cm^{-1}.

Figure 7 shows scanning electron microscopy (SEM) images of a "square-diamond" pattern and the edge of the same pattern. The squares in the "square-diamond" pattern are ablated with a pulse train of 200 fs laser pulses at a rate of 250 kHz with a pulse energy of 40 nJ. The squares are well-defined, with a minimum amount of debris. These SEM images were obtained after the samples were cleaned for 10 min in methanol in an ultrasonic cleaner in order to remove any debris from the ablation process. The samples were then sputter coated with a thin layer of gold to provide conductivity for SEM examination.

Figure 8 shows a typical micro-Raman spectrum of an irradiated area of a laser-processed synthetic LPCVD diamond sample after debris removal which confirms the removal of the graphitized traces in the focus of the laser beam. This combined system rules out possible imprecisions coming from the use of the two independent techniques, in addition to avoiding significant time associated with sample repositioning and beam realignment and refocusing. The method avoids the need to move the sample under test from one workstation to a separate measuring station or the need to change the beam path of the pumping laser or the train of femtosecond pulses. It only requires turning the microscope revolving turret to change over from femtosecond machining to conventional Raman spectroscopy (and usually only some fine focusing) or vice versa.

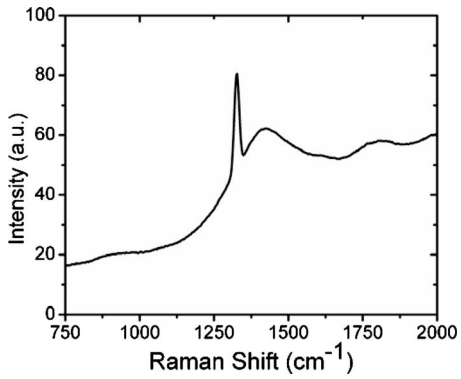

FIG. 8. A typical micro-Raman spectrum of an irradiated area of a laser-processed synthetic LPCVD diamond sample after debris removal. It exhibits the characteristic single line near 1332 cm^{-1} and background peaks above ~1400 cm^{-1}.

The attractiveness of integrating Raman spectroscopy with femtosecond laser ablation is a result of technological improvements. The large gain in sensitivity, speed of spectral acquisition, and the improvement in signal-to-noise ratio resulting from new hardware and techniques permits Raman spectroscopy to be applied to a wide range of samples of practical importance. Much of the stimulus for the renewed development of analytical Raman spectroscopy is the ease and versatility of sampling modes and the high spectral information content.[10] Further progress can be expected with the next generations of femtosecond laser systems on the market.

Femtosecond laser oscillators delivering just nanojoules of energy per pulse can be employed in laser micromachining using NAs close to or larger than unity.[18] In the present system, this can be achieved by using the "oscillator only" output (Fig. 1). To achieve submicron scale machining precision, not only must the laser pulses be of femtosecond duration and near threshold, they must also be focused with high NA microscope objectives.[18,19] Furthermore, care must be taken to ensure that the laser is focused to a diffraction limited spot size. The geometry of the final structure in single shot ablations can be influenced by the pulse intensity and the NA. The latter determines the width of the focal volume and therefore the resulting feature size. For NAs larger than 0.6, the micromachined features are almost spherically symmetric; below this value, the resulting structures become larger and asymmetric. Changing the spatial profile and divergence of the input beam prior to focusing, such that the focal-spot profile is closer to a symmetric circular cross section, can mitigate the asymmetry.[20,21] For pulse duration greater than 10 ps as in our case, the threshold intensity varies as the square root of the pulse duration. The relatively small effect of altering pulse duration on the threshold intensity provides flexibility in the choice of laser system, which is important for commercial applications of femtosecond laser micromachining.[22]

IV. SUMMARY

We have introduced a newly developed integrated system for micro-/nanofemtosecond machining and Raman spectroscopy, which is the first of its kind. Combining micro-/nanofemtosecond machining with Raman spectroscopy provides a powerful tool for materials modification and

analysis. In addition to creating features on various materials, the experimental setup allows micro-Raman measurements to be carried out on the exact path used for the ablation while carefully coordinating the alignment and positioning of these features through software-controlled stages with nanometer precision.

The integrated scanning microscope is a new advance that is robust, flexible, easy to modify, and allows us to improve functionality. Furthermore, it decreases experimental complexity and increases sampling reliability. This is important particularly when dealing with very small samples or very small sampled areas of transparent or opaque materials, single crystals, and other small particles. The integrated scanning microscope is well within the capabilities and budgets of most educational institutions and includes a digital imaging capability valuable to capture digital images for femtosecond machining for educational, research, or archival purposes. It is also a precise focusing aid and is important for proper sample location and to monitor the progress of the operation.

The utility of the combined system is demonstrated using diamond materials. The diamond samples in this study are irradiated with 200 fs pulses of 800 nm wavelength. The pulse repetition rate is 250 kHz. In the focal region of the irradiated pulses, the diamond is transformed to graphite in the form of debris. The removal of debris removes the graphitized traces in the focus of the laser beam. These examples are important for applications such as industrial research and analysis of the femtosecond ablation involving diamond.

ACKNOWLEDGMENTS

Tom Smith, President of Diamond Edge Co., furnished the synthetic single crystal diamond samples. The authors acknowledge funding from the Tennessee Higher Education Commission through the Center for Laser Applications at University of Tennessee Space Institute. Mr. Douglas K. Warnberg is acknowledged for valuable technical input.

[1] *Recent Advances In Laser Processing of Materials*, edited by J. Perriere, E. Millon, and E. Fogarassy (Elsevier, New York, 2006).
[2] *3D Laser Microfabrication: Principles and Applications*, edited by H. Misawa and S. Juodkazis (Wiley-VCH Verlag GmbH & Co. KGaA, Weinheim, 2006).
[3] *Laser Ablation and Its Applications*, edited by C. Phipps (Springer, New York, 2007).
[4] E. Mazur, Proceedings of the Conference On Lasers and Electro-Optics Europe, Munich, Germany, 2009.
[5] G. Kamlage, T. Bauer, A. Ostendorf, and B. N. Chichkov, Appl. Phys. A: Mater. Sci. Process. **77**, 307 (2003).
[6] D. A. Long, *The Raman Effect: A Unified Treatment of the Theory of Raman Scattering by Molecules* (Wiley, New York, 2002).
[7] *Modern Techniques in Raman Spectroscopy*, edited by J. J. Laserna (Wiley, New York, July 1996).
[8] *Infrared and Raman Spectroscopy: Methods and Applications*, edited by B. Schrader (VCH, Weinberim, 1995).
[9] E. Smith and G. Dent, *Modern Raman Spectroscopy: A Practical Approach* (Wiley, Chichester, 2005).
[10] *Raman Spectroscopy for Chemical Analysis*, edited by J. D. Winefordner (Wiley-Interscience, New York, 2000), Vol. 157.
[11] G. Turrell and P. Dhamelincourt, in *Modern Techniques in Raman Spectroscopy*, edited by J. J. Laserna (Wiley, New York, 1996).
[12] R. O. Dillon, J. A. Woollam, and V. Katkanant, Phys. Rev. B **29**, 3482 (1984).
[13] A. C. Ferrari and J. Robertson, Phys. Rev. B **61**, 14095 (2000).
[14] *Tribology of Diamond-Like Carbon Films: Fundamentals and Applications*, edited by C. Donnet and A. Erdemir (Springer, New York, 2007), Vol. 1.
[15] T. V. Kononenko, M. S. Komlenok, V. P. Pashinin, S. M. Pimenov, V. I. Konov, M. Neff, V. Romano, and W. Luthy, Diamond Relat. Mater. **18**, 196 (2009).
[16] *RegA Model 9000 Laser Operator's Manual* (Coherent, Inc., Santa Clara, 1997), Part Number 0165-083-00, Rev B.
[17] R. Le Harzic, H. Schuck, D. Sauer, T. Anhut, I. Riemann, and K. Konig, Opt. Express **13**, 6651 (2005).
[18] C. B. Schaffer, A. Brodeur, J. F. Garcia, and E. Mazur, Opt. Lett. **26**, 93 (2001).
[19] C. B. Schaffer and E. Mazur, Opt. Photonics News **12**, 20 (2001).
[20] G. H. Cheng, Y. S. Wang, Q. Liu, W. Zhao, and G. F. Chen, Acta Phys. Sin. **53**, 436 (2004).
[21] R. Osellame, J. Opt. Soc. Am. B **20**, 1559 (2003).
[22] N. Bloembergen, IEEE J. Sel. Top. Quantum Electron. **10**, 375 (1974).